João F. S. Trentin
Departamento de Engenharia Mecânica,
Faculdade de Engenharia
UNESP - Universidade Estadual Paulista,
Ilha Solteira, SP 15385-000, Brasil
e-mail: joao.trentin@unesp.br

Samuel da Silva
Departamento de Engenharia Mecânica,
Faculdade de Engenharia
UNESP - Universidade Estadual Paulista,
Ilha Solteira, SP 15385-000, Brasil
e-mail: samuel.silva13@unesp.br

Hanspeter Schaub
Department of Aerospace Engineering Sciences,
Colorado Center for Astrodynamics Research,
University of Colorado Boulder,
Boulder, CO 80309-0431
e-mail: hanspeter.schaub@colorado.edu

Variable Speed Control Moment Gyroscope in an Inverted Pendulum

The use of variable speed control moment gyroscope (VSCMG) is an effective way for attitude stabilization of aerospace devices. It is possible to control the oscillation and direction rate of change in rigid bodies in space due to the controlled change of angular momentum rate. Thus, this paper proposes an atypical pendulum configuration controlled by a VSCMG actuator. The idea of the VSCMG pendulum (VSCMGP) is to use both the angular momentum variation in amplitude and direction to implement the control. The controller is designed using Lyapunov theory to stabilize the pendulum in the inverted position. The results illustrate the control using a VSCMG in an inverted pendulum showing how the stabilization of an inverted pendulum is performed using two control actions. Also, the comparison of the proposed pendulum with a classical configuration is presented. [DOI: 10.1115/1.4044273]

Keywords: reaction wheel, pendulum, nonlinear control, nonlinear dynamics, variable speed control moment gyroscope—VSCMG

1 Introduction

The attitude control of aerospace devices has some challenges to be overcome, for example, complex nonlinear motion equations, uncertainties, and disturbances that occur during operation. Reaction wheels can be applied in other fields and in particular in the control and stabilization of mechanisms due to its simple configuration and its reliability to aerospace industry applications [1–4]. This class of actuator is very common in systems that require attitude change, and it can store angular momentum, which may aid in stabilization and external disturbances torques rejection. The most usual way to use a reaction wheel to produce torque is from the angular velocity variation causing an angular momentum variation in amplitude. In this scenario, it is possible, from specific angular velocities, to control the oscillation and direction rate of rigid bodies in space through the application of torques in the reaction wheel. The fundamental physical principle consists of the validity of the conservation of the angular momentum and the equilibrium of its rate of variation with the involved torques [5–11].

In particular, different types of pendulums can be tested and controlled using reaction wheels as actuators [12–14]. Additionally, the use of inverted pendulums to approximate the dynamics of robots has been extensively studied [13–27]. For instance, the introduction of the reaction mass pendulum, in which a three-dimensional multibody pendulum has represented well the model of a humanoid robot with variable body inertia [13,14], and many other different configurations of inverted three-dimensional pendulums have encouraged the development of control for humanoids [15,16,19–21,25]. There are also other approximations of pendulum configurations that represent different types of robots, such as the wheeled inverted pendulum [17,22–24,27]. However, to the best of our knowledge, an inverted pendulum has not been controlled using the variable speed control moment gyroscope (VSCMG) yet. In this way, *control moment gyroscope*—CMG is a widely known form of control that has many applications, such as the attitude control of aerospace devices, as satellites [28–33], robots [34], and spacecraft [35,36]. There are also other uses of a CMG, such as a personal balance assistance [37,38], for example. A simple CMG consists of a rotating disk in a constant rate and in a gimbal mechanism that can change its direction generating a gyroscopic torque by the direction variation of angular momentum [39,40]. CMGs have the advantage of a small angular variation in the gimbal producing a high magnitude torque in the device to be controlled [39]. However, CMGs with a constant speed in the reaction wheel can present singularities in some specific angular positions and then they may not be so effective. Therefore, to avoid such singularities Schaub et al. [39] discuss the VSCMG in which the favorable aspects of using reaction wheels are combined with CMGs. In this case, the reaction wheel angular velocity can be adjusted and controlled for situations in which singularities can occur and the gyroscopic torque can also be applied [39–42]. For this reason, the VSCMG is a suitable method to control an inverted pendulum with a reaction wheel.

In this sense, the main idea and contribution of this paper are to propose a new configuration of a pendulum with a VSCMG mechanism coupled to it. The control torque is produced by the reaction wheel and by the gyroscopic effect when the reaction wheel is gimbaled, driving the pendulum from the downward position to the inverted position. This paper is organized as follows: Sec. 2 presents the dynamic modeling of the new pendulum configuration proposed. Section 3 shows the design of the controller using Lyapunov control theory, and Sec. 4 shows the numerical results for driving the pendulum to the inverted position and also when it is subject to an external disturbance. Additionally, the comparison with a well-known pendulum configuration, the reaction wheel pendulum (RWP), is carried out. Finally, Sec. 5 shows the concluding remarks of the paper and future work.

2 Dynamic Modeling

Figure 1 illustrates three frames used for modeling the variable speed control moment gyroscope coupled to a pendulum. The inertial frame is described by axes (x, y, z) and orthonormal basis $\{\hat{n}_1, \hat{n}_2, \hat{n}_3\}$. The first moving frame (B), or body frame, is described by axes (x_1, y_1, z_1), and the orthonormal basis

Contributed by the Dynamic Systems Division of ASME for publication in the Journal of Dynamic Systems, Measurement, and Control. Manuscript received July 25, 2018; final manuscript received July 12, 2019; published online September 18, 2019. Assoc. Editor: Ming Xin.

$\{\hat{b}_1, \hat{b}_2, \hat{b}_3\}$ is rotating solidarity to the pendulum with the angle θ, assuming a negative rotation. The second moving frame (G), or gimbal frame, is described by axes (x_2, y_2, z_2) and orthonormal basis $\{\hat{g}_t, \hat{g}_g, \hat{g}_s\}$. This frame is responsible for rotating the gimbal with angle γ, which makes the reaction wheel move outside of the plane; and for rotating the gimbal, a positive rotation is considered. The rotation matrix between the inertial frame and moving frame B is described by

$$\begin{Bmatrix} \hat{b}_1 \\ \hat{b}_2 \\ \hat{b}_3 \end{Bmatrix} = \underbrace{\begin{bmatrix} \cos\theta & -\sin\theta & 0 \\ \sin\theta & \cos\theta & 0 \\ 0 & 0 & 1 \end{bmatrix}}_{[BN]} \begin{Bmatrix} \hat{n}_1 \\ \hat{n}_2 \\ \hat{n}_3 \end{Bmatrix} \tag{1}$$

The rotation matrix between the body moving frame B and the gimbal moving frame G is given by

$$\begin{Bmatrix} \hat{g}_t \\ \hat{g}_g \\ \hat{g}_s \end{Bmatrix} = \underbrace{\begin{bmatrix} \cos\gamma & 0 & -\sin\gamma \\ 0 & 1 & 0 \\ \sin\gamma & 0 & \cos\gamma \end{bmatrix}}_{[BG]^{\mathrm{T}}} \begin{Bmatrix} \hat{b}_1 \\ \hat{b}_2 \\ \hat{b}_3 \end{Bmatrix} \tag{2}$$

In this new system there are three different angular velocities to be evaluated: the pendulum angular velocity ${}^{B}\boldsymbol{\omega}_{B/N} = \dot{\theta}\,\hat{b}_3$, the gimbal angular velocity ${}^{B}\boldsymbol{\omega}_{G/B} = \dot{\gamma}\,\hat{b}_2$, and the reaction wheel angular velocity ${}^{B}\boldsymbol{\omega}_{W/G} = \dot{\psi}\sin\gamma\,\hat{b}_1 + \dot{\psi}\cos\gamma\,\hat{b}_3$. In this way, the inertial angular wheel velocity is ${}^{B}\boldsymbol{\omega}_{W/N} = \dot{\psi}\cos\gamma\,\hat{b}_1 + \dot{\gamma}\,\hat{b}_2 + (\dot{\theta} + \dot{\psi}\cos\gamma)\,\hat{b}_3$.

Before calculating the angular momentum, it is necessary to compute the inertia matrix. This is done for the pendulum, for the gimbal, and the reaction wheel. The principal inertia directions of the gimbal and the reaction wheel are in a different frame. So, it is necessary to rotate these inertia matrices to the body frame B, where the VSCMG pendulum is adequately modeled. The pendulum inertia matrix in the body moving frame B is

$${}^{B}[I_p] = \begin{bmatrix} I_{p_x} & 0 & 0 \\ 0 & I_{p_y} & 0 \\ 0 & 0 & I_{p_z} \end{bmatrix} = \begin{bmatrix} I_p & 0 & 0 \\ 0 & 0 & 0 \\ 0 & 0 & I_p \end{bmatrix} \tag{3}$$

where $I_{p_x} = I_{p_z} = (ml^2/3) = I_p$ and $I_{p_y} = 0$, since for the pendulum the inertia of a rod was considered. For the gimbal inertia matrix, it is necessary to rotate it to the body frame B. The inertia matrix of the gimbal in the gimbal frame is given by

$${}^{G}[I_g] = \begin{bmatrix} I_{gt} & 0 & 0 \\ 0 & I_{gg} & 0 \\ 0 & 0 & I_{gs} \end{bmatrix} \tag{4}$$

moreover, the inertia matrix of the gimbal in the body frame B is

$$\begin{aligned} {}^{B}[I_g] &= [BG][I_g][BG]^{\mathrm{T}} \\ &= \begin{bmatrix} I_{gs}\sin^2\gamma + I_{gt}\cos^2\gamma & 0 & (I_{gs} - I_{gt})\cos\gamma\sin\gamma \\ 0 & I_{gg} & 0 \\ (I_{gs} - I_{gt})\cos\gamma\sin\gamma & 0 & I_{gt}\sin^2\gamma + I_{gs}\cos^2\gamma \end{bmatrix} \end{aligned} \tag{5}$$

where $[BG]$ is the rotation matrix between the body and gimbal frame. It is worth noting that the reaction wheel is symmetric, and the principal inertia directions of the gimbal and the reaction wheel are equivalent. The inertia matrix of the reaction wheel can be written in the gimbal moving frame G

$${}^{G}[I_W] = \begin{bmatrix} I_{wt} & 0 & 0 \\ 0 & I_{wt} & 0 \\ 0 & 0 & I_{ws} \end{bmatrix} \tag{6}$$

Finally, the inertia matrix of the reaction wheel in the body frame is

$$\begin{aligned} {}^{B}[I_W] &= [BG][I_W][BG]^{\mathrm{T}} \\ &= \begin{bmatrix} I_{ws}\sin^2\gamma + I_{wt}\cos^2\gamma & 0 & (I_{ws} - I_{wt})\cos\gamma\sin\gamma \\ 0 & I_{wt} & 0 \\ (I_{ws} - I_{wt})\cos\gamma\sin\gamma & 0 & I_{wt}\sin^2\gamma + I_{ws}\cos^2\gamma \end{bmatrix} \end{aligned} \tag{7}$$

The total angular momentum of the system (${}^{B}\boldsymbol{H}$) is the sum of the angular momentum of the pendulum (${}^{B}\boldsymbol{H}_B$), of the gimbal (${}^{B}\boldsymbol{H}_G$) and the reaction wheel (${}^{B}\boldsymbol{H}_W$), given by

$${}^{B}\boldsymbol{H} = {}^{B}\boldsymbol{H}_B + {}^{B}\boldsymbol{H}_G + {}^{B}\boldsymbol{H}_W \tag{8}$$

that can be rewritten as

$${}^{B}\boldsymbol{H} = {}^{B}[I_p]\,{}^{B}\boldsymbol{\omega}_{B/N} + {}^{B}[I_g]\,{}^{B}\boldsymbol{\omega}_{G/N} + {}^{B}[I_W]\,{}^{B}\boldsymbol{\omega}_{W/N} \tag{9}$$

where ${}^{B}\boldsymbol{\omega}_{G/N} = {}^{B}\boldsymbol{\omega}_{B/N} + {}^{B}\boldsymbol{\omega}_{G/B}$. The time derivative of the angular momentum in frame B taken relative to the inertial frame N is

$$\dot{\boldsymbol{H}} = \frac{{}^{N}\mathrm{d}}{\mathrm{dt}}\boldsymbol{H} = \frac{{}^{B}\mathrm{d}}{\mathrm{dt}}({}^{B}\boldsymbol{H}) + {}^{B}\boldsymbol{\omega}_{B/N} \times {}^{B}\boldsymbol{H} = {}^{B}\boldsymbol{L} \tag{10}$$

Finally, the motion equation is obtained by

$$\mathcal{A}\ddot{\theta} + \mathcal{B}\ddot{\psi} + \mathcal{C}\dot{\gamma} + \mathcal{D} = 0 \tag{11}$$

where

$$\mathcal{A} = I_{wt}\sin^2\gamma + I_{ws}\cos^2\gamma + I_p + I_{gt}\sin^2\gamma + I_{gs}\cos^2\gamma \tag{12}$$

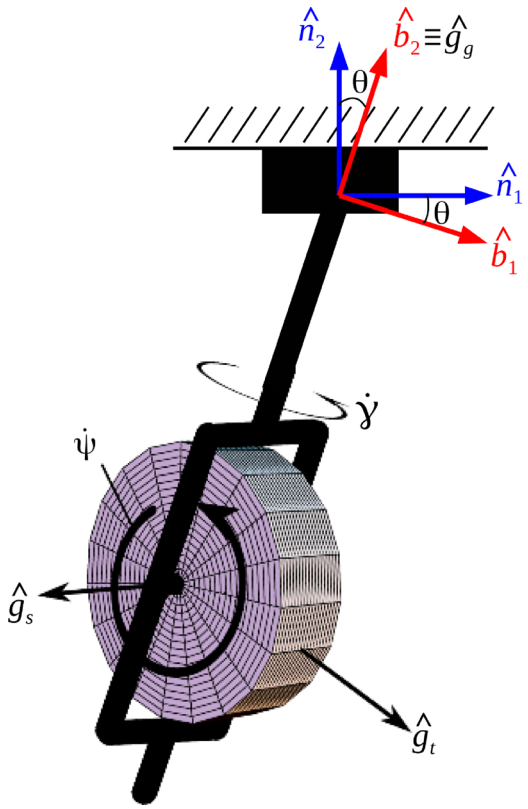

Fig. 1 VSCMG pendulum

$$\mathcal{B} = I_{ws}\cos\gamma \tag{13}$$

$$\mathcal{C} = \dot{\theta}\cos\gamma\sin\gamma(2I_{wt} + 2I_{gt} - 2I_{ws} - 2I_{gs}) - \dot{\psi}I_{ws}\sin\gamma \tag{14}$$

$$\mathcal{D} = -rmg\sin\theta \tag{15}$$

The motor torque equation for the gimbal is obtained by analyzing it separately from the whole system. This can be done in the body frame or the gimbal frame. However, if it is carried out in the gimbal frame, it is not required to rotate the gimbal matrix, which leads to simpler equations. Thus, the angular momentum used to obtain the motor torque equation for the gimbal is

$$^{G}\boldsymbol{H}_{GW} = {}^{G}[I_g]\,{}^{G}\boldsymbol{\omega}_{G/N} + {}^{G}[I_W]\,{}^{G}\boldsymbol{\omega}_{W/N} \tag{16}$$

The motor torque equation of the gimbal can be obtained by performing the following derivation of the angular momentum of the gimbal and the reaction wheel in the gimbal frame, G, relative to the inertial frame, N

$$\dot{\boldsymbol{H}}_{GW} = \frac{^{N}\mathrm{d}}{\mathrm{dt}}\boldsymbol{H}_{GW} = \frac{^{G}\mathrm{d}}{\mathrm{dt}}\left({}^{G}\boldsymbol{H}_{GW}\right) + {}^{G}\boldsymbol{\omega}_{G/N}\times{}^{G}\boldsymbol{H}_{GW} = {}^{G}\boldsymbol{L}_{GW} \tag{17}$$

Thus, Eq. (18) is the motor torque equation for the gimbal, where u_g is the control torque produced by the gimbal

$$u_g = (I_{gg} + I_{wt})\ddot{\gamma} + I_{ws}\dot{\psi}\dot{\theta}\sin\gamma \tag{18}$$

It is also essential to analyze the reaction wheel separately to obtain its motor torque equation. As the direction in which this torque is produced is $\hat{g}_s$, it is more convenient to perform the analysis in the gimbal frame. The angular momentum for the reaction wheel is

$$^{G}\boldsymbol{H}_{W} = {}^{G}[I_W]\,{}^{G}\boldsymbol{\omega}_{W/N} \tag{19}$$

By performing the derivation of the angular momentum of the reaction wheel in the gimbal frame G relative to the inertial frame N

$$\dot{\boldsymbol{H}}_{W} = \frac{^{N}\mathrm{d}}{\mathrm{dt}}\boldsymbol{H}_{W} = \frac{^{G}\mathrm{d}}{\mathrm{dt}}\left({}^{G}\boldsymbol{H}_{W}\right) + {}^{G}\boldsymbol{\omega}_{G/N}\times{}^{G}\boldsymbol{H}_{W} = {}^{G}\boldsymbol{L}_{W} \tag{20}$$

the following reaction wheel motor torque equation is obtained:

$$u_s = I_{ws}\ddot{\theta}\cos\gamma - I_{ws}\dot{\theta}\dot{\gamma}\sin\gamma + I_{ws}\ddot{\psi} \tag{21}$$

where u_s is the control torque provided by the reaction wheel. The simultaneous numerical integration of Eqs. (11), (18), and (21) provides the motion of the VSCMG pendulum. Regarding the notations, see Ref. [10].

3 Nonlinear Control

First, it is necessary to select a candidate to be a Lyapunov function to design a feedback control law using the Lyapunov control theory

$$\mathcal{V}(\delta\theta, \delta\dot{\theta}) = \frac{\delta\dot{\theta}^2}{2} + K\frac{\delta\theta^2}{2} \tag{22}$$

where $\delta\dot{\theta} = \dot{\theta} - \dot{\theta}_r$, $\delta\theta = \theta - \theta_r$, and K is a scalar attitude feedback gain. To ensure stability, the derivative of the Lyapunov candidate function should be at least negative semidefinite, as

$$\dot{\mathcal{V}}(\delta\theta, \delta\dot{\theta}) = \delta\dot{\theta}(\delta\ddot{\theta} + K\delta\theta) \tag{23}$$

In this way, $\dot{\mathcal{V}}(\delta\theta, \delta\dot{\theta})$ is set to be equal to a negative definite function, in this case

$$\dot{\mathcal{V}}(\delta\theta, \delta\dot{\theta}) = \delta\dot{\theta}(\delta\ddot{\theta} + K\delta\theta) = -P\delta\dot{\theta}^2 \tag{24}$$

By carrying out the derivative of the Lyapunov candidate function, it is possible to obtain the following stable closed-loop dynamical system:

$$\ddot{\theta} - \ddot{\theta}_r + P\delta\dot{\theta} + K\delta\theta = 0 \tag{25}$$

To find the control law, it is necessary to substitute the equation of motion of the system into the closed-loop system. Nonetheless, it is necessary to analyze the higher-order derivatives of the Lyapunov candidate function in order to find out which kind of stability it ensures [43]

$$\ddot{\mathcal{V}}(\delta\theta, \delta\dot{\theta}) = -2P\delta\dot{\theta}\delta\ddot{\theta}; \quad \ddot{\mathcal{V}}(\delta\theta, \delta\dot{\theta} = 0) = 0 \tag{26}$$

So, it is essential to analyze the third derivative of $\mathcal{V}(\delta\theta, \delta\dot{\theta})$

$$\dddot{\mathcal{V}}(\delta\theta, \delta\dot{\theta}) = -2P\delta\ddot{\theta}^2 - 2P\delta\dot{\theta}\dddot{\theta} \tag{27}$$

$$\dddot{\mathcal{V}}(\delta\theta, \delta\dot{\theta} = 0) = -2P\delta\ddot{\theta}^2 \tag{28}$$

Analyzing $\dot{\mathcal{V}}(\delta\theta, \delta\dot{\theta} = 0)$ when

$$\delta\dot{\theta}(\delta\ddot{\theta} + K\delta\theta) = -P\delta\dot{\theta}^2 \tag{29}$$

$$\delta\ddot{\theta} + K\delta\theta = -P\delta\dot{\theta} \tag{30}$$

$$\delta\ddot{\theta} = -K\delta\theta \tag{31}$$

Substituting the result presented in Eq. (31) into Eq. (28)

$$\dddot{\mathcal{V}}(\delta\theta, \delta\dot{\theta} = 0) = -2P\delta(-K\delta\theta)^2 = -2PK^2\delta\theta^2 < 0 \tag{32}$$

The third derivative of $\mathcal{V}(\delta\theta, \delta\dot{\theta})$ is negative definite, and because the first nonzero $\mathcal{V}$ derivative is of odd order, the control law is asymptotically stable.

3.1 Control Law. By substituting the motion equation shown in Eq. (11) into the closed-loop dynamics presented in Eq. (25) and solving for the desired control vector

$$[\mathcal{B}\quad \mathcal{C}]\begin{Bmatrix}\ddot{\psi}\\ \dot{\gamma}\end{Bmatrix} = -\mathcal{D} - \mathcal{A}\ddot{\theta}_r + P\mathcal{A}\delta\dot{\theta} + K\mathcal{A}\delta\theta = \boldsymbol{L}_r \tag{33}$$

The control law given by Eq. (33) can avoid many of the conventional CMG singularities once that the RW rotor speed is time-varying [10]. The state vector $\boldsymbol{\eta} = \{\ddot{\psi}\quad \dot{\gamma}\}^T$ and the matrix $[Q] = [\mathcal{B}\ \mathcal{C}]$ are used to simplify the notation. Thus, the steering law presented in Eq. (33) can be rewritten as

$$[Q]\boldsymbol{\eta} = \boldsymbol{L}_r \tag{34}$$

The inverse of $[Q]$ matrix is computed to find the rates for the reaction wheel and the gimbal. This can be done using the standard Moore–Penrose inverse to obtain a minimum norm solution. However, assuming that a VSCMG should act as a classical CMG away from singular configurations, a weighted pseudo-inverse is used [44]. For the case of the VSCMG pendulum, $[W]$ is a diagonal matrix

$$[W] = \begin{bmatrix} W_w & 0\\ 0 & W_g\end{bmatrix} \tag{35}$$

where W_w and W_g are the weights related to the reaction wheel and gimbal modes, respectively; these weights represent how

active each mode is. The desired $\boldsymbol{\eta}$ can be found as done in Schaub et al. [39]

$$\boldsymbol{\eta} = \begin{Bmatrix} \ddot{\psi} \\ \dot{\gamma} \end{Bmatrix} = [W][Q]^{\mathrm{T}} \left([Q][W][Q]^{\mathrm{T}} \right)^{-1} \boldsymbol{L}_r \tag{36}$$

To obtain the required performance from the VSCMG, the weights are estimated to see how close to a single-gimbal singularity the VSCMG is. By computing the nondimensional scalar factor δ, the proximity of the singularity can be evaluated as below:

$$\delta = \frac{1}{h^2} \left([\mathcal{C}][\mathcal{C}]^{\mathrm{T}} \right) \tag{37}$$

where h is the RW nominal angular momentum. If the parameter δ goes to zero, this indicates a singular configuration for the CMG. The weight W_w can be defined as

$$W_w = W_w^o e^{-\mu\delta} \tag{38}$$

The parameters W_w^o and μ are positive scalars to be chosen by the designer. When the VSCMG is operating away from singularities, it should behave as a CMG, i.e., the weights on the reaction wheel mode are smaller than the one from the CMG mode. The weight of W_g is held constant.

3.2 Torque Level Control Law. It is important to obtain a torque level control command for the system that is being studied since the steering law presented in Eq. (33) provides only kinematic directive. It is necessary to investigate a subservo control law for the VSCMG pendulum steering law, i.e., develop the control for $\ddot{\psi}$ and $\dot{\gamma}$.

To evaluate the motor torque u_g, the gimbal angular acceleration $\ddot{\gamma}$ is needed. So, it is necessary to develop a feedback control to obtain an expression for $\ddot{\gamma}$ to yield a stable servodynamics. To develop the gimbal rate servo, it is essential to determine $\ddot{\gamma}$ such that the actual gimbal rate $\dot{\gamma}$ approaches the desired gimbal $\dot{\gamma}_d$ that is determined through the VSCMG steering law presented in Eq. (33). The servotracking error is defined as

$$\Delta\dot{\gamma} = \dot{\gamma} - \dot{\gamma}_d \tag{39}$$

and the Lyapunov function selected is

$$\mathcal{V}(\Delta\dot{\gamma}) = \frac{1}{2}\Delta\dot{\gamma}^2 \tag{40}$$

where this function is a positive definite measure of the servotracking error. Evaluating the time derivative of the Lyapunov function and forcing it to be definite negative leads to

$$\dot{\mathcal{V}}(\Delta\dot{\gamma}) = \Delta\dot{\gamma}\Delta\ddot{\gamma} \equiv -K_\gamma \Delta\dot{\gamma}^2 \tag{41}$$

with $K_\gamma > 0$. Solving Eq. (41) for the desired gimbal acceleration yields

$$\ddot{\gamma} = \ddot{\gamma}_d - K_\gamma \Delta\gamma \tag{42}$$

The feedforward term $\ddot{\gamma}_d$ may be evaluated by numerically differentiating the desired gimbal steering law rates $\dot{\gamma}_d$. Substituting Eq. (42) into Eq. (18) leads to the gimbal rate servo control torque

$$u_g = (I_{gg} + I_{wt})(\ddot{\gamma}_d - K_\gamma \Delta\gamma) + I_{ws}\dot{\psi}\dot{\theta}\sin\gamma \tag{43}$$

A servo for the reaction wheel acceleration control is also developed similarly. Let $\ddot{\psi}_d$ be the desired reaction wheel acceleration that results from the steering law presented in Eq. (33). The speed tracking error for the reaction wheel is

$$\Delta\dot{\psi} = \dot{\psi} - \dot{\psi}_d \tag{44}$$

As done before for the gimbal, the following Lyapunov function is chosen

$$\mathcal{V}(\Delta\dot{\psi}) = \frac{1}{2}\Delta\dot{\psi}^2 \tag{45}$$

This function is also a definite positive measure of the servotracking error. The time derivative of the Lyapunov function for the reaction wheel feedback control is evaluated, and it is forced to be definite negative, leading to

$$\dot{\mathcal{V}}(\Delta\dot{\psi}) = \Delta\dot{\psi}\Delta\ddot{\psi} \equiv -K_\psi \Delta\dot{\psi}^2 \tag{46}$$

with $K_\psi > 0$, the following is obtained

$$\ddot{\psi} = \ddot{\psi}_d - K_\psi \Delta\dot{\psi} \tag{47}$$

such that the new reaction wheel torque control is given by

$$u_s = I_{ws}\left(\ddot{\psi}_d - K_\psi \Delta\dot{\psi} \right) + I_{ws}\ddot{\theta}\cos\gamma - I_{ws}\dot{\theta}\dot{\gamma}\sin\gamma \tag{48}$$

4 Numerical Results

This section shows the results obtained to control the VSCMG pendulum in the inverted position. How this new system and its controller react when the pendulum is subjected to external disturbances after controlled in the inverted position is also presented.

For the VSCMG pendulum, a reaction wheel with radius $R = 0.11$ m, mass $m_w = 0.2151$ kg, a pendulum length of $\ell = 0.35$ m with a mass of $m_p = 0.1$ kg are considered. The gimbal structure has a mass equal to $m_g = 0.082$ kg, and its inertia was obtained using SOLIDWORKS, where $I_{gt} = 0.0020441\ \mathrm{kg/m^2}$, $I_{gg} = 0.0020466\ \mathrm{kg/m^2}$, and $I_{gs} = 0.0000054\ \mathrm{kg/m^2}$. The radius of the center of mass is $r = \left(m_g\ell/2 + m_g\ell + m_w\ell\right)/(m_p + m_g + m_w)$. The following initial conditions for all the simulations were assumed to be $\theta(0) = 180$ deg, $\dot{\theta}(0) = 0$, $\psi(0) = 0$, $\dot{\psi}(0) = 100$ rpm, $\gamma(0) = 90$ deg and $\dot{\gamma}(0) = 0$.

For the controller designed, the gains used in the simulations were $K = 5$, $P = 5$, $K_\gamma = 100$, and $K_\psi = 100$. The weights for the controller were $W_w = 2$, $W_g = 1$, and $\mu = 10^{-9}$. In the control algorithm, first, the initial conditions are set, i.e., the angular position where it is intended to control the pendulum ($\theta = 0$ deg) and the controller parameters. Afterward, $\boldsymbol{L}_r$ is obtained, such that the desired rates for the gimbal and the reaction wheel can be obtained. With these desired rates, the motor torques of the gimbal (u_g) and the reaction wheel (u_s) can be evaluated. Then, the integration of the complete model is performed, and the new states are obtained.

Furthermore, the proposed inverted pendulum configuration with a VSCMG is compared with the classical and well-known RWP. The model of the RWP has been described in many papers, and one can notice that if we lock the gimbal at $\gamma = 0$ deg, the VSCMGP becomes the classical RWP. This can also be addressed in the equations that describe the motion of the system. Considering $\gamma = 0$ deg, the equation of motion of VSCMG pendulum becomes

$$(I_{ws} + I_p + I_{gs})\ddot{\theta} + (I_{ws})\ddot{\psi} + \mathcal{D} = 0 \tag{49}$$

The motor torque of the gimbal yields zero since the gimbal has to be locked in the RWP. Moreover, the motor torque of the reaction wheel becomes

$$u_s = I_{ws}\ddot{\theta} + I_{ws}\ddot{\psi} \tag{50}$$

Equations (49) and (50) are the exact same equations of the RWP that were proposed by Spong et al. [12] and describe its motion.

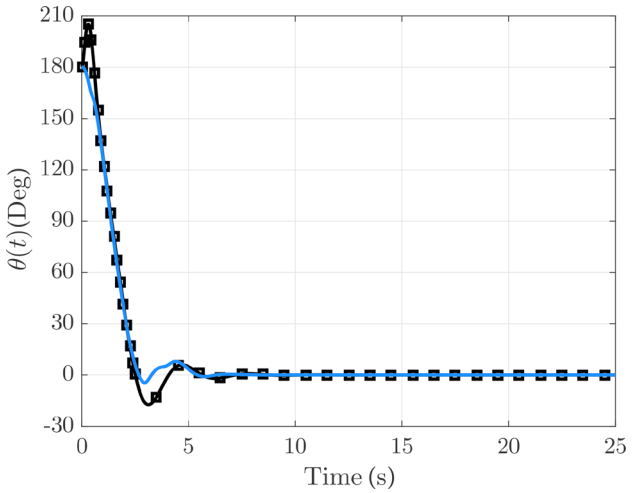

Fig. 2 Pendulum angular position $\theta(t)$, where — indicates the result for VSCMGP and –□– indicates the result for RWP

For the simulations of the RWP, the same parameters presented were used; the only difference is that the weight of the gimbal mode W_g in the controller is set to be zero, since that for the RWP the reaction wheel is not gimballed.

4.1 Numerical Results for Controlling the Pendulums in the Inverted Position. Figure 2 presents the results for driving the VSCMG pendulum and RWP from the downward position ($\theta = 180$ deg) to the upward position ($\theta = 0$ deg). The pendulum angular position for both configurations is close but the VSCMG seems to have a better outcome.

Figure 3 depicts the gimbal rates for both systems studied. For the RWP, the gimbal rate must be zero for all the simulation, as observed. Analyzing the VSCMG pendulum, the gyroscopic torque is more used in the beginning of the simulation to start moving the pendulum, and after some seconds, the torque is mainly produced by the reaction wheel. Some differences between the desired gimbal rate and the effective gimbal rate for the VSCMG can be noticed because for the CMG torque u_g, a saturation limit of 2.5 N·m has been added, which makes the control more realistic.

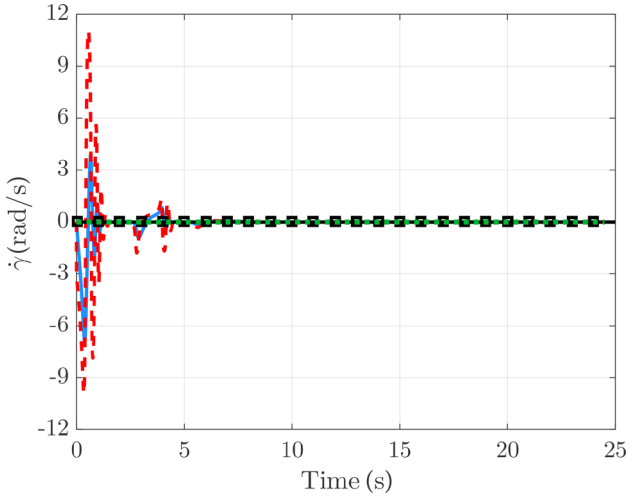

Fig. 3 Gimbal rate $\dot{\gamma}(t)$. — indicates the effective gimbal rate, and - - - indicates the desired gimbal rate for the VSCMGP. –□– indicates the effective gimbal rate, and ····· indicates the desired gimbal rate for the RWP.

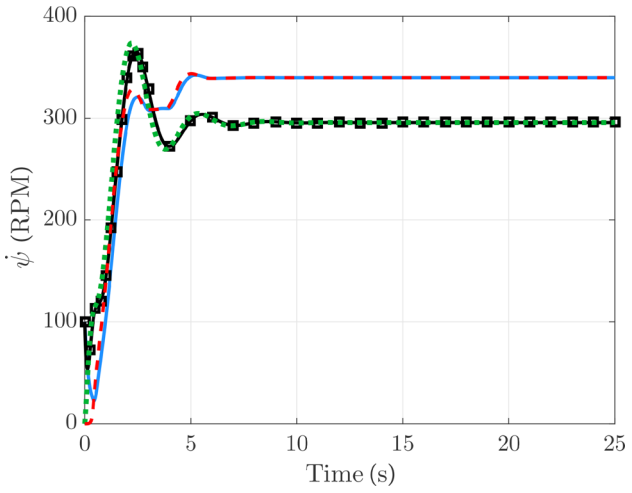

Fig. 4 RW angular velocity $\dot{\psi}(t)$. — indicates the effective reaction wheel angular velocity, and - - - indicates the desired reaction wheel angular velocity for the VSCMGP. –□– indicates the effective reaction wheel angular velocity, and ····· indicates the desired reaction wheel angular velocity for the RWP.

For both pendulum configurations, the reaction wheel angular velocities are shown in Fig. 4, where after the pendulum reaches the equilibrium in the inverted position the wheel speed is constant, for all cases.

Additionally, the angular velocity of the reaction wheel of the RWP reaches a higher value in the beginning of the simulation; this occurs because in the RWP the torque is provided only by the reaction wheel mode, and it does not have the contribution of the CMG mode.

Figure 5 shows the contribution of each control action for the VSCMG pendulum and the external torque caused by gravity. In addition, the angular momentum variation can also be observed. Here, the gyroscopic torque has a higher contribution in the start of the simulation, and after some time, the control is performed mainly by the reaction wheel mode.

Figure 6 shows the control actions, the external torque caused by gravity and the variation of angular momentum for the RWP. The gimbal control action is kept at zero, as expected, since the

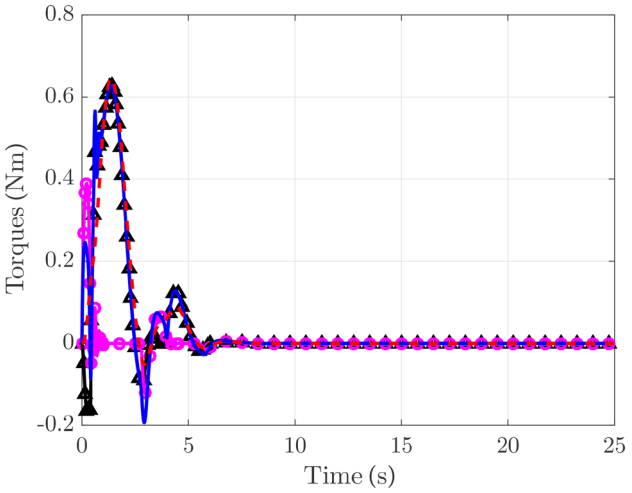

Fig. 5 Control actions and torques. - - - indicates the external torque caused by gravity ($\mathcal{D}$), - indicates the composition of the angular momentum variation ($\dot{H}_3 = \mathcal{A}\ddot{\theta} + \mathcal{B}\ddot{\psi} + \mathcal{C}\dot{\gamma}$), -△- indicates the reaction wheel control action ($\mathcal{B}\ddot{\psi}$) and -○- indicates the CMG control action ($\mathcal{C}\dot{\gamma}$)

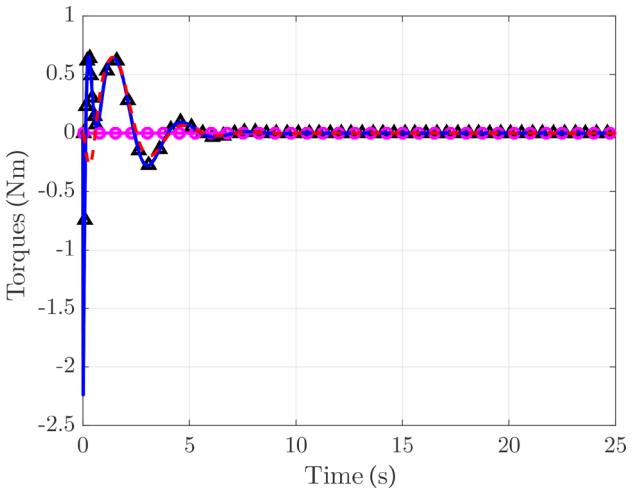

Fig. 6 Control actions and torques. - - - indicates the external torque caused by gravity ($\mathcal{D}$), - indicates the composition of the angular momentum variation ($\dot{H}_3 = \mathcal{A}\ddot{\theta} + \mathcal{B}\ddot{\psi} + \mathcal{C}\ddot{\gamma}$), -△- indicates the reaction wheel control action ($\mathcal{B}\ddot{\psi}$) and -○- indicates the CMG control action ($\mathcal{C}\ddot{\gamma}$)

Table 1 RMS of the control actions

	Inverted		Disturbance	
Action	VSCMGP	RWP	VSCMGP	RWP
$\mathcal{B}\ddot{\psi}$	0.1345	0.1706	0.1631	0.2230
$\mathcal{C}\ddot{\gamma}$	0.0418	0	0.0459	0

gimbal is not actuated for this configuration. Thus, the control is performed only by the reaction wheel control action.

In this way, a higher action from the reaction wheel is necessary in the beginning of the simulation. When analyzing the VSCMG pendulum in Fig. 5, this is not observed because the actions are distributed between the gimbal and reaction wheel. The RMS values of the control actions of VSCMG pendulum and RWP were calculated, and they are presented in Table 1, where the comparison between pendulum configurations is discussed.

Figure 7 shows the angular momentum component around $\hat{b}_3$ for both pendulums, where after the pendulum is controlled in the inverted position, it becomes a constant value, as expected, because when the pendulum is balanced in the inverted position gravity does not cause a torque, illustrating the conservation of the angular momentum. This result is observed for both pendulum configurations.

4.2 Numerical Results for Controlling the Pendulums in the Inverted Position With an External Disturbance. Other simulations were done when an external disturbance is applied after the pendulum is controlled in the inverted position. Also, we investigate how the RWP would react when subjected to a disturbance so that this situation can also be compared between the pendulum configurations. For all the simulations in this section, the disturbance was applied at 12 s for 0.5 s with an amplitude of $D_{\text{ist}} = 0.3$ N·m. So, for this case, the pendulums angular positions are presented in Fig. 8 where at approximately 12 s both pendulums are removed from the equilibrium position due to the disturbances applied to the systems.

It is also interesting to note that the controller designed can bring both pendulums back to the desired position ($\theta = 0$ deg) after these systems are subjected to an external disturbance. However, comparing the results between the VSCMG pendulum and the RWP, the angular displacement of the VSCMGP is slightly smaller, which means that the system that employs two control actions reacts better when subjected to a disturbance, whereas the RWP angular displacement reaches a higher value. Since these results are still close to each other, the performance indexes were calculated for this situation, and they are presented in Table 2 showing that the VSCMG pendulum presented a better performance than the RWP.

Figure 9 shows the gimbal rates ($\dot{\gamma}$) for both pendulums, where for the VSCMG pendulum the gimbal is used in the beginning of the simulation and also when the disturbance is applied. Again, there is a difference between the desired rate and the actual gimbal rate due to the saturation limit imposed on the CMG torque (u_g). For the RWP, the desired and effective gimbal rate is zero since for this configuration the gimbal must be locked and the torques must be generated only by the reaction wheel. This result can be observed in Fig. 9, where the gimbal rate for the RWP is also presented.

Figure 10 shows the angular velocities of the reaction wheels for both systems. After the disturbances are applied, the controller needs to accelerate the reaction wheel to produce torque to compensate for the disturbance applied to the pendulums. Since for the RWP the torque is produced only by the reaction wheel, it demands a higher acceleration for the reaction wheel to be able to deal with the disturbance applied, whereas for the VSCMG

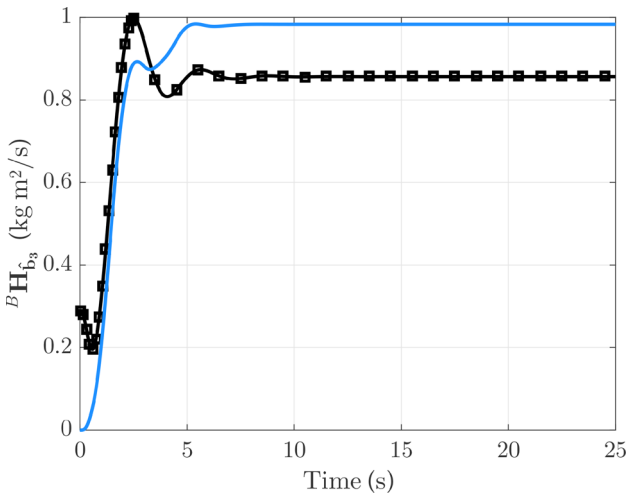

Fig. 7 Angular momentum $^B\boldsymbol{H}$ around $\hat{\boldsymbol{b}}_3$, where — indicates the result for VSCMGP and –□– indicates the result for RWP

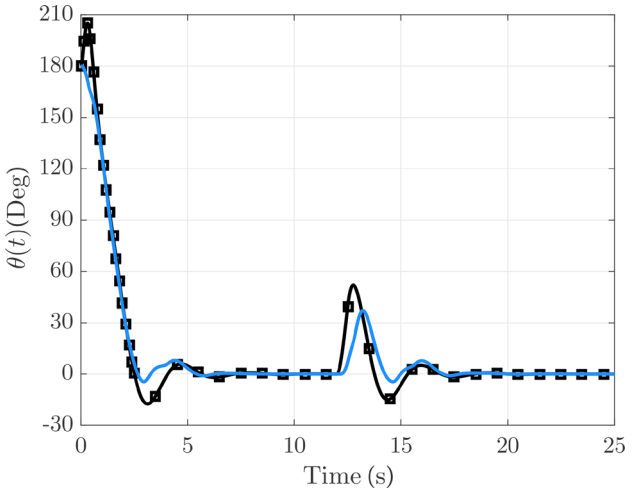

Fig. 8 Pendulum angular position $\theta(t)$ when subject to external disturbance, where — indicates the result for VSCMGP and –□– indicates the result for RWP

Table 2 Performance indexes calculated to compare both pendulum configurations

	Inverted		Disturbance	
Index	VSCMGP	RWP	VSCMGP	RWP
ISE	10.09	12.01	10.42	12.65
IAE	4.57	5.10	5.44	6.34
ITAE	4.60	5.57	16.66	22.49
ITSE	6.57	7.58	10.92	15.92

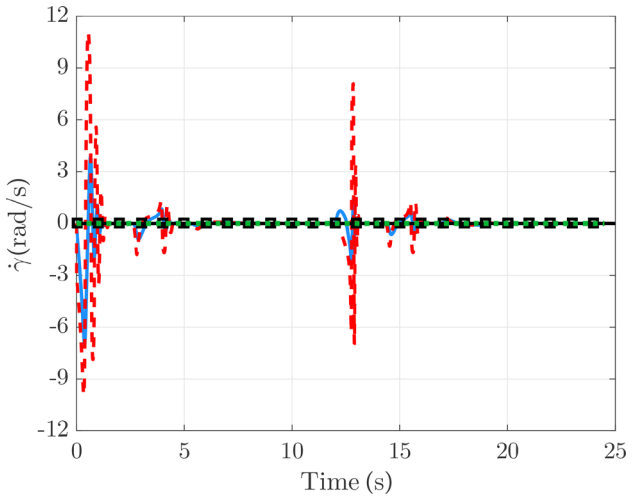

Fig. 9 Gimbal rate $\dot{\gamma}(t)$ when subject to an external disturbance. — indicates the effective gimbal rate and - - - indicates the desired gimbal rate for the VSCMGP. –□– indicates the effective gimbal rate and ····· indicates the desired gimbal rate for the RWP.

pendulum this acceleration is smaller, due to the fact that the gyroscopic contribution is also added.

Analyzing the contribution of each control action presented in Fig. 11 for the VSCMG pendulum subjected to a disturbance after being controlled in the inverted position, both modes are used to deal with the disturbance applied to the system even if a higher value for the weight of the wheel mode (W_w) is considered

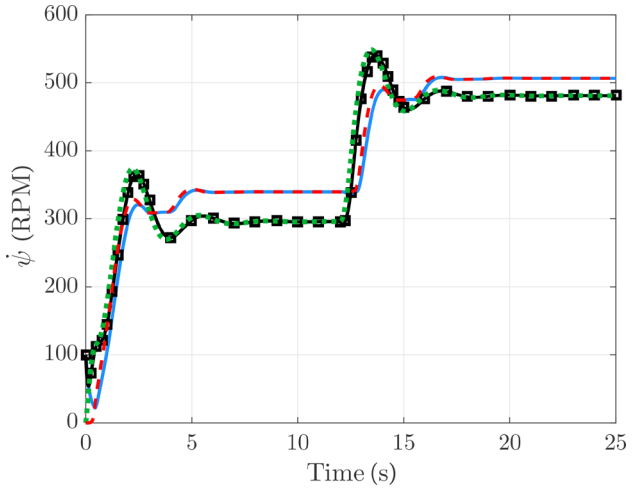

Fig. 10 RW angular velocity $\dot{\psi}(t)$ when subject to external disturbance. — indicates the effective reaction wheel angular velocity and - - - indicates the desired reaction wheel angular velocity for the VSCMGP. –□– indicates the effective reaction wheel angular velocity and ····· indicates the desired reaction wheel angular velocity for the RWP.

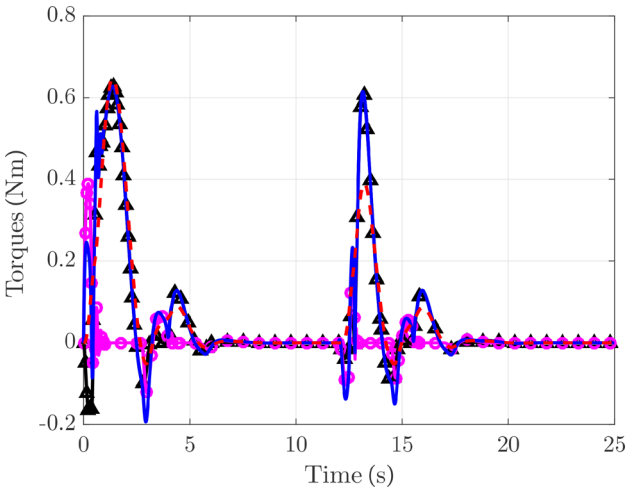

Fig. 11 Control actions and torques when subject to external disturbance. - - - indicates the external torque caused by gravity ($\mathcal{D}$), - indicates the composition of the angular momentum variation ($\dot{H}_3 = \mathcal{A}\ddot{\theta} + \mathcal{B}\ddot{\psi} + \mathcal{C}\dot{\gamma}$), -△- indicates the reaction wheel control action ($\mathcal{B}\ddot{\psi}$) and -○- indicates the CMG control action ($\mathcal{C}\dot{\gamma}$)

compared to the one related to the gimbal mode (W_g). However, both control actions help to control the pendulum by employing the gyroscopic torque and the torque produced by the reaction wheel.

Figure 12 presents the control actions for the RWP. Here, just the reaction wheel control action is used to control the inverted pendulum, and there is no contribution from the gyroscopic torque since the gimbal is locked for this case.

Since only one control action is used, the values reached by this action are higher than the ones obtained for the VSCMG pendulum presented in Fig. 11. The RMS values for the control actions for the RWP were calculated, and they are presented in Table 1 to be compared with the ones for the VSCMG pendulum, when these systems are subjected to an external disturbance.

Figure 13 presents the angular momentum around $\hat{b}_3$ for both systems, illustrating the change in the angular momentum after the disturbance is applied. The conservation of the angular momentum can also be seen since the pendulum was controlled in

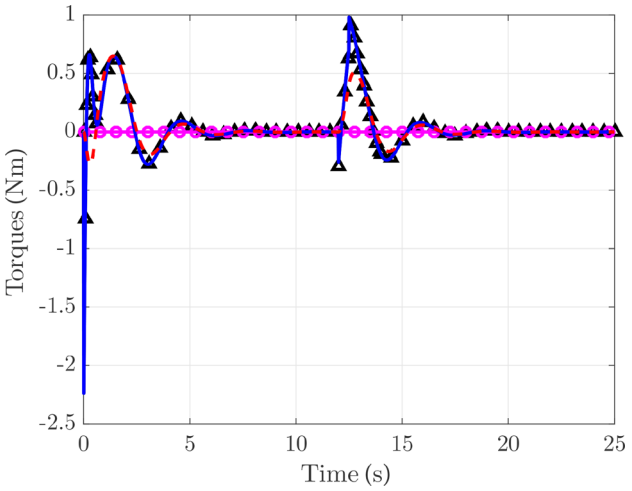

Fig. 12 Control actions and torques when subject to external disturbance. - - - indicates the external torque caused by gravity ($\mathcal{D}$), - indicates the composition of the angular momentum variation ($\dot{H}_3 = \mathcal{A}\ddot{\theta} + \mathcal{B}\ddot{\psi} + \mathcal{C}\dot{\gamma}$), -△- indicates the reaction wheel control action ($\mathcal{B}\ddot{\psi}$) and -○- indicates the CMG control action ($\mathcal{C}\dot{\gamma}$)

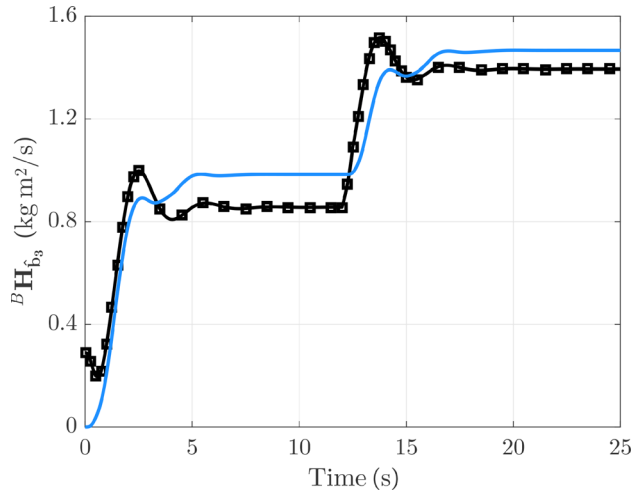

Fig. 13 Angular momentum $^B\boldsymbol{H}$ around $\hat{\boldsymbol{b}}_3$ when subject to external disturbance, where — indicates the result for VSCMGP and –□– indicates the result for RWP

the inverted position; then, a disturbance was applied; at last, the angular pendulum position was controlled again, and the angular momentum was conserved once again.

4.3 Comparison Between Performances. This section presents a detailed analysis of the performance of the two pendulum systems analyzed. This comparison is conducted to evaluate how the new configuration proposed performs when confronted to an existing one.

The results presented in Figs. 2 and 8 for the angular pendulum position considering the two situations of both pendulum configurations analyzed in this paper were close. Therefore, four performance indexes were calculated to evaluate the results for controlling the angular pendulum position of the systems studied. Usually, these indexes are minimized during the design of the controller to guarantee the best performance, but they can also be used to analyze the resulting performance of systems. The system that presents the smaller indexes is the system with the best performance. The first index evaluated was the integral of time multiplied by the absolute error (ITAE), given by

$$\text{ITAE} = \int_0^T t|e(t)|dt \tag{51}$$

where t is time, and $|e(t)|$ is the absolute error. The other index calculated was the integral of the square of the error (ISE)

$$\text{ISE} = \int_0^T e(t)^2 dt \tag{52}$$

where $e(t)$ is the error. The integral of the absolute magnitude of the error (IAE) was the third index evaluated

$$\text{IAE} = \int_0^T |e(t)|dt \tag{53}$$

The fourth index is the integral of time multiplied by the square error (ITSE)

$$\text{ITSE} = \int_0^T te(t)^2 dt \tag{54}$$

The use of more than one index was applied to verify if, with other metrics, the same result for the analysis of the performance is obtained. Each index has a different characteristic, for example, the ITAE emphasizes the steady-state error, and the IAE is commonly used to analyze computational simulations, among other reasons [45]. The values of the indexes are presented in Table 2. For both cases studied in this paper (that is, in the inverted position and subjected to a disturbance) with the parameters chosen, the VSCMG pendulum outperforms the RWP configuration.

Moreover, the RMS value of the control actions presented in Figs. 5, 6, 11, and 12 is evaluated. The RMS value of a generic signal (x_{rms}) is given by

$$x_{\text{rms}} = \sqrt{\frac{1}{n}\left(x_1^2 + x_2^2 + \cdots + x_n^2\right)} \tag{55}$$

Thereby, the RMS of the reaction wheel control action and the gimbal control action were calculated for the two situations analyzed in this paper for both pendulum configurations. The RMS values obtained are presented in Table 1.

Analyzing the RMS values obtained, the VSCMG pendulum had lower values for the reaction wheel control action since for such configuration the control actions are divided into two. For the RWP, the control is performed only by the reaction wheel control action, and for both cases, the RMS values obtained were higher than the ones from the VSCMG. This indicates that the RWP had higher energy consumption.

5 Final Remarks

This paper presented a new configuration of a pendulum that has a VSCMG mechanism stabilized in the inverted position. A nonlinear controller using the Lyapunov control theory was designed to perform the position control of this new configuration. Thus, the use of two control actions, gyroscopic torque and the torque provided by the reaction wheel, was beneficial to drive the pendulum from the downward position to its upward position, thus controlling it in the unstable equilibrium point. Additionally, when this new system was subjected to an external disturbance, the controller designed was able to return the pendulum to the desired position by employing both control actions. Also, the reaction wheel mode is more used than the CMG mode due to the fact that the pendulum motion is restricted to the plane. Moreover, the comparison between the VSCMG pendulum with a well-established configuration in the literature, the reaction wheel pendulum, was carried out. The results of the comparison have shown that for the cases studied in this paper, the proposed pendulum configuration had a better performance. So, future work includes the study of an inverted spherical pendulum with a VSCMG mechanism to assess more complex situations.

Acknowledgment

The authors are thankful to the anonymous reviewers and the Associate Editor for their relevant comments and useful suggestions.

Funding Data

- São Paulo Research Foundation (FAPESP) (Grant Nos. 2016/21997-0, 2017/12985-2, and 2018/13751-8; Funder ID: 10.13039/501100001807).
- Brazilian National Council for Scientific and Technological Development (CNPq) (Grant No. 307520/2016-1; Funder ID: 10.13039/501100003593).

Nomenclature

$[BN]$ = rotation matrix between frames B and N
$[BG]^T$ = rotation matrix between frames B and G
$\dot{\boldsymbol{H}}$ = time derivative of the angular momentum in the body frame B taken relative to the inertial frame N
$\dot{\boldsymbol{H}}_{GW}$ = time derivative of the angular momentum of the gimbal and reaction wheel in the gimbal frame G taken relative to the inertial frame N

$\dot{\boldsymbol{H}}_W$ = time derivative of the angular momentum of the reaction wheel in the gimbal frame G taken relative to the inertial frame N
${}^B\boldsymbol{H}$ = angular momentum of the system in the body frame B
${}^B\boldsymbol{H}_B$ = angular momentum of the pendulum in the body frame B
${}^B\boldsymbol{H}_G$ = angular momentum of the gimbal in the body frame B
${}^B\boldsymbol{H}_W$ = angular momentum of the reaction wheel in the body frame B
${}^G\boldsymbol{H}_{GW}$ = angular momentum of the gimbal and reaction wheel in the gimbal frame G
${}^G\boldsymbol{H}_W$ = angular momentum of the reaction wheel in the gimbal frame G
${}^B[I_p]$ = pendulum inertia matrix in the body frame B
${}^B[I_g]$ = gimbal inertia matrix in the body frame B
${}^B[I_W]$ = reaction wheel inertia matrix in the body frame B
${}^B\boldsymbol{\omega}_{B/N}$ = pendulum angular velocity in frame B relative to inertial frame N
${}^B\boldsymbol{\omega}_{G/B}$ = gimbal angular velocity in frame G relative to body frame B
${}^B\boldsymbol{\omega}_{W/G}$ = reaction wheel angular velocity in frame W relative to gimbal frame G
${}^B\boldsymbol{\omega}_{W/N}$ = reaction wheel angular velocity in frame W relative to inertial frame N

References

[1] Rui, C., Kolmanovsky, I. V., and McClamroch, N. H., 2000, "Nonlinear Attitude and Shape Control of Spacecraft With Articulated Appendages and Reaction Wheels," IEEE Trans. Autom. Control, **45**(8), pp. 1455–1469.
[2] Nudehi, S. S., Farooq, U., Alasty, A., and Issa, J., 2008, "Satellite Attitude Control Using Three Reaction Wheels," American Control Conference (ACC), Seattle, WA, June 11–13, pp. 4850–4855.
[3] Jepsen, F., Soborg, A., Pedersen, A. R., and Yang, Z., 2009, "Development and Control of an Inverted Pendulum Driven by a Reaction Wheel," International Conference on Mechatronics and Automation (ICMA), Changchun, China, Aug. 9–12, pp. 2829–2834.
[4] Ismail, Z., and Varatharajoo, R., 2010, "A Study of Reaction Wheel Configurations for a 3-Axis Satellite Attitude Control," Adv. Space Res., **45**(6), pp. 750–759.
[5] Sperry, E. A., 1913, "Engineering Applications of the Gyroscope," J. Franklin Inst., **175**(5), pp. 447–482.
[6] Deimel, R. F., 1950, *Mechanics of the Gyroscope: The Dynamics of Rotation*, Dover, Mineola, NY.
[7] Scarborough, J. B., 1958, *The Gyroscope: Theory and Applications*, Interscience Publishers, Geneva, Switzerland.
[8] Cannon, R. H., 1967, *Dynamics of Physical Systems*, McGraw-Hill, New York.
[9] Whittaker, E., and McCrae, W., 1988, *A Treatise on the Analytical Dynamics of Particles and Rigid Bodies*. Cambridge Mathematical Library, Cambridge University Press, New York.
[10] Schaub, H., and Junkins, J. L., 2014, *Analytical Mechanics of Space Systems*, 3rd ed., AIAA Education Series, Reston, VA.
[11] Goldstein, H., Poole, C. P., and Safko, J., 2011, *Classical Mechanics*, 9th ed., Pearson, New York.
[12] Spong, M. W., Corke, P., and Lozano, R., 2001, "Nonlinear Control of the Reaction Wheel Pendulum," Automatica, **37**(11), pp. 1845–1851.
[13] Lee, S.-H., and Goswami, A., 2007, "Reaction Mass Pendulum (RMP): An Explicit Model for Centroidal Angular Momentum of Humanoid Robots," IEEE International Conference on Robotics and Automation (ICRA), Rome, Italy, Apr. 10–14, pp. 4667–4672.
[14] Sanyal, A. K., and Goswami, A., 2013, "Dynamics and Balance Control of the Reaction Mass Pendulum: A Three-Dimensional Multibody Pendulum With Variable Body Inertia," ASME J. Dyn. Syst., Meas., Control, **136**(2), p. 021002.
[15] Kajita, S., Kanehiro, F., Kaneko, K., Yokoi, K., and Hirukawa, H., 2001, "The 3D Linear Inverted Pendulum Mode: A Simple Modeling for a Biped Walking Pattern Generation," IEEE/RSJ International Conference on Intelligent Robots and Systems, Maui, HI, Oct. 29–Nov. 3, pp. 239–246.
[16] Sugihara, T., Nakamura, Y., and Inoue, H., 2002, "Real-Time Humanoid Motion Generation Through Zmp Manipulation Based on Inverted Pendulum Control," IEEE International Conference on Robotics and Automation (ICRA'02), Washington, DC, May 11–15, pp. 1404–1409.
[17] Grasser, F., D'Arrigo, A., Colombi, S., and Rufer, A. C., 2002, "Joe: A Mobile, Inverted Pendulum," IEEE Trans. Ind. Electron., **49**(1), pp. 107–114.
[18] Furuta, K., 2003, "Control of Pendulum: From Super Mechano-System to Human Adaptive Mechatronics," 42nd IEEE International Conference on Decision and Control (CDC), Maui, HI, Dec. 9–12, pp. 1498–1507.
[19] Kajita, S., Kanehiro, F., Kaneko, K., Fujiwara, K., Harada, K., Yokoi, K., and Hirukawa, H., 2003, "Resolved Momentum Control: Humanoid Motion Planning Based on the Linear and Angular Momentum," IEEE/RSJ International Conference on Intelligent Robots and Systems (IROS 2003), Las Vegas, NV, Oct. 27–31, pp. 1644–1650.
[20] Kajita, S., Morisawa, M., Miura, K., Nakaoka, S., Harada, K., Kaneko, K., Kanehiro, F., and Yokoi, K., 2010, "Biped Walking Stabilization Based on Linear Inverted Pendulum Tracking," IEEE/RSJ International Conference on Intelligent Robots and Systems (IROS), Taipei, Taiwan, Oct. 18–22, pp. 4489–4496.
[21] Tsai, Y.-Y., Lin, W.-C., Cheng, K. B., Lee, J., and Lee, T.-Y., 2010, "Real-Time Physics-Based 3D Biped Character Animation Using an Inverted Pendulum Model," IEEE Trans. Visualization Comput. Graphics, **16**(2), pp. 325–337.
[22] Yang, C., Li, Z., Cui, R., and Xu, B., 2014, "Neural Network-Based Motion Control of an Underactuated Wheeled Inverted Pendulum Model," IEEE Trans. Neural Networks Learn. Syst., **25**(11), pp. 2004–2016.
[23] Vasudevan, H., Dollar, A. M., and Morrell, J. B., 2015, "Design for Control of Wheeled Inverted Pendulum Platforms," ASME J. Mech. Rob., **7**(4), p. 041005.
[24] Jeong, S., and Hayashi, T., 2018, "Development of a Wheeled Inverted Pendulum Mobile Platform With a Four-Bar Parallel Mechanism," Adv. Rob., **32**(4), pp. 191–201.
[25] Liu, C., Ning, J., and Chen, Q., 2018, "Dynamic Walking Control of Humanoid Robots Combining Linear Inverted Pendulum Mode With Parameter Optimization," Int. J. Adv. Rob. Syst., **15**(1), epub.
[26] An, K., Liu, Y., Li, Y., Zhang, Y., and Liu, C., 2018, "Energetic Walking Gaits Studied by a Simple Actuated Inverted Pendulum Model," J. Mech. Sci. Technol., **32**(5), pp. 2273–2281.
[27] He, C., Huang, K., Chen, X., Zhang, Y., and Zhao, H., 2018, "Transportation Control of Cooperative Double-Wheel Inverted Pendulum Robots Adopting Udwadia-Control Approach," Nonlinear Dyn., **91**(4), pp. 2789–2802.
[28] Bailey, D. A., 2000, "CMG Control Based on Angular Momentum to Control Satellite Attitude," U.S. Patent No. 6,128,556.
[29] Bailey, D. A., 2000, "Orienting a Satellite With Controlled Momentum Gyros," U.S. Patent No. 6,154,691.
[30] Han, C., and Pechev, A. N., 2007, "Underactuated Satellite Attitude Control With Two Parallel CMGS," IEEE International Conference on Control and Automation (ICCA), Guangzhou, China, May 30–June 1, pp. 666–670.
[31] MacKunis, W., Dupree, K., Bhasin, S., and Dixon, W., 2008, "Adaptive Neural Network Satellite Attitude Control in the Presence of Inertia and CMG Actuator Uncertainties," American Control Conference (ACC), Seattle, WA, June 11–13, pp. 2975–2980.
[32] Clark, C., Worrall, K., and Yavuzoğlu, E., 2010, "A Control Moment Gyro for Dynamic Attitude Control of Small Satellites," 24th Annual AIAA/USU Conference on Small Satellites, Logan, UT, Aug. 9–12, Paper No. SSC10-XI-8.
[33] Noumi, A., and Takahashi, M., 2013, "Fault-Tolerant Attitude Control Systems for a Satellite Equipped With Control Moment Gyros," AIAA Paper No. 2013-5119.
[34] Senda, K., Murotsu, Y., Nagaoka, H., and Mitsuya, A., 1995, "Attitude Control for Free-Flying Space Robot With CMG (Control Moment Gyroscopes)," AIAA Paper No. 95-3336-CP.
[35] Roser, X., and Sghedoni, M., 1997, "Control Moment Gyroscopes (CMG's) and Their Application in Future Scientific Missions," Third ESA International Conference on Spacecraft Guidance, Navigation and Control Sustems, Noordwijk, The Netherlands, Nov. 26–29, pp. 523–528.
[36] Omagari, K., Fujihashi, K., and Matunaga, S., 2008, "CMG Configuration and Control for Rapid Attitude Maneuver of Small Spacecraft," Ninth International Symposium on Artificial Intelligence, Robotics and Automation in Space, Hollywood, Feb. 26–29, pp. 26–29.
[37] Berry, A., Lemus, D., Babuška, R., and Vallery, H., 2016, "Directional Singularity-Robust Torque Control for Gyroscopic Actuators," IEEE/ASME Trans. Mechatronics, **21**(6), pp. 2755–2763.
[38] Lemus, D., van Frankenhuyzen, J., and Vallery, H., 2017, "Design and Evaluation of a Balance Assistance Control Moment Gyroscope," ASME J. Mech. Rob., **9**(5), p. 051007.
[39] Schaub, H., Vadali, S. R., and Junkins, J. L., 1998, "Feedback Control Law for Variable Speed Control Moment Gyros," J. Astronaut. Sci., **46**(3), pp. 307–328.
[40] Schaub, H., and Junkins, J. L., 2000, "Singularity Avoidance Using Null Motion and Variable-Speed Control Moment Gyros," J. Guid., Control, Dyn., **23**(1), pp. 11–16.
[41] McMahon, J., and Schaub, H., 2009, "Simplified Singularity Avoidance Using Variable-Speed Control Moment Gyroscope Null Motion," J. Guid., Control, Dyn., **32**(6), pp. 1938–1943.
[42] Stevenson, D., and Schaub, H., 2012, "Nonlinear Control Analysis of a Double-Gimbal Variable-Speed Control Moment Gyroscope," J. Guid., Control, Dyn., **35**(3), pp. 787–793.
[43] Mukherjee, R., and Chen, D., 1993, "Asymptotic Stability Theorem for Autonomous Systems," J. Guid., Control, Dyn., **16**(5), pp. 961–963.
[44] Junkins, J. L., 1978, *An Introduction to Optimal Estimation of Dynamical Systems*, **3**, Kluwer Academic Pub, Dordrecht, The Netherlands.
[45] Dorf, R. C., and Bishop, R. H., 2011, *Modern Control Systems*, Pearson, New York.